CRYSTAL GROWTH & DESIGN
2009
VOL. 9, NO. 8
3626–3631

Vanadium Pentoxide Nanostructures: An Effective Control of Morphology and Crystal Structure in Hydrothermal Conditions

Waldir Avansi Jr.,*[,†] Cauê Ribeiro,[‡] Edson R. Leite,[§] and Valmor R. Mastelaro[†]

Instituto de Física de São Carlos, Universidade de São Paulo, São Carlos, SP, Brazil, Embrapa, Empresa Brasileira de Pesquisas Agropecuárias, São Carlos, SP, Brazil, and LIEC- DQ/UFSCAR, Universidade Federal de São Carlos, São Carlos, SP, Brazil

Received April 5, 2009; Revised Manuscript Received May 4, 2009

ABSTRACT: A systematic study was made of the synthesis of $V_2O_5 \cdot nH_2O$ nanostructures, whose morphologies, crystal structure, and amount of water molecules between the layered structures were regulated by strictly controlling the hydrothermal treatment variables. The synthesis involved a direct hydrothermal reaction between V_2O_5 and H_2O_2, without the addition of organic surfactant or inorganic ions. The experimental results indicate that high purity nanostructures can be obtained using this simple and clean synthetic route. On the basis of a study of hydrothermal treatment variables such as reaction temperature and time, X-ray diffraction (XRD) and scanning transmission electron microscopy (STEM) revealed that it was possible to obtain nanoribbons of the $V_2O_5 \cdot nH_2O$ monoclinic phase and nanowires or nanorods of the $V_2O_5 \cdot nH_2O$ orthorhombic phase. Thermal gravimetric analysis (TGA) shows also that the water content in the structure can be controlled at appropriate hydrothermal conditions. Concerning the oxidation state of the vanadium atoms of as-obtained samples, a mixed-valence state composed of V^{4+} and V^{5+} was observed in the $V_2O_5 \cdot nH_2O$ monoclinic phase, while the valence of the vanadium atoms was preferentially 5+ in the $V_2O_5 \cdot nH_2O$ orthorhombic phase. The X-ray absorption near-edge structure (XANES) results also indicated that the local structure of vanadium possessed a higher degree of symmetry in the $V_2O_5 \cdot nH_2O$ monoclinic phase.

Introduction

In the past decade, nanostructured vanadium oxide compounds have attracted much interest due to their chemical and physical properties and their great potential for applications in catalysis,[1,2] as sensors,[3−5] in electrochromic devices,[6,7] in electrochemistry,[8−10] in photocatalytic activities,[10] and in spintronic devices.[11] Among the various vanadium oxide compositions that can be obtained, vanadium pentoxide (V_2O_5) possesses a unique set of properties and is one of the most widely studied of the more stable phases of vanadium oxides.[12,13] Because its structure is composed of two-dimensional layers, this material is also used as an intercalation compound.[2,12] The literature offers several reports of interesting results, concerning applications for the hydrated form of vanadium pentoxide ($V_2O_5 \cdot nH_2O$).[2,3,9−19] The different applications of $V_2O_5 \cdot nH_2O$ nanoparticles are related directly to the amount of water molecules (n) between the layers and to their morphology.[2,3,10,11,18] According to Livage et al.,[15] the amount n in $V_2O_5 \cdot nH_2O$ nanoribbons is related directly to the amount of V^{4+} ions, and the distance between the layers, d, depends on this amount of n.

V_2O_5 nanoparticles have been obtained through various methods such as sol−gel,[12] reverse-micelle,[23,24] or quenching in water.[21,25] The sol−gel method, which is one of the methods most widely used to obtain V_2O_5 nanoparticles, is considered time-consuming because samples generally take several days to be formed. Several recent papers describe a sol−gel method followed by hydrothermal treatment to prepare different vanadium oxide compounds.[26,27] Hydrothermal treatments make it possible to obtain different morphologies, which are dependent on the synthesis route.[3,10,28−31] Li et al. obtained different $V_2O_5 \cdot nH_2O$ nanostructures by a hydrothermal route using NH_4VO_3 as the raw material in the presence of different acids. According to these authors, the morphology and compositions depend on acids used to control the pH value, and that the morphology and composition of the synthesized products had an evident influence on the electrochemical intercalation properties and photocatalytic activities.[10] Also, using NH_4VO_3 as the precursor and HNO_3 to control the pH, Pan et al. [29] obtained $V_2O_5 \cdot 0.3H_2O$ nanowires with a small fraction of $V_2O_5 \cdot nH_2O$ ($0.3 < n < 1.7$) and V_2O_5 phases. Using a similar synthetic route, Liu et al. obtained $V_2O_5 \cdot nH_2O$ materials through hydrothermal treatment at 180 °C for 24 h. By thermally treating $V_2O_5 \cdot nH_2O$ materials at 400 °C, they obtained a V_2O_5 orthorhombic phase with nanowire morphology. These authors demonstrated that their $V_2O_5 \cdot nH_2O$ samples were more sensitive to ethanol at a low concentration (<10 ppm), while V_2O_5 nanowires showed a higher sensitivity to high ethanol concentrations.[3] Zhou et al. also obtained orthorhombic V_2O_5 nanowires by a hydrothermal method, using $VOSO_4 \cdot nH_2O$ as a precursor and $KBrO_3$ as an oxidant. They demonstrated that only between 160−180 °C, with a controlled pH value and in the presence of a strong oxidant such as $KBrO_3$, could they supply the necessary driving force to remove H_2O molecules embedded in the layered structure of $V_2O_5 \cdot nH_2O$.[30] Some studies have also shown that the morphology of these nanoparticles can be controlled by using appropriate organic molecules as templates.[27]

Many researchers have recently focused on routes based on the reaction between V_2O_5 and hydrogen peroxide (H_2O_2), which has proved to be an "easy" and "clean" methodology to obtain $V_2O_5 \cdot nH_2O$ nanoparticles.[12,19,20] This method excludes the presence of foreign ions or organic ligands and offers an accurate way to control the vanadium concentration.[12] Alonso et al. reported on an NMR study of $V_2O_5 \cdot nH_2O$ gel obtained reacting V_2O_5 with H_2O_2. They showed that the dissolution of V_2O_5 by hydrogen peroxide leads to the formation of unstable diperoxo $[VO(O_2)_2]^-$ species in the solution. This species decomposes to form $[VO(O_2)]^+$ species and subsequently vanadate species,

* Corresponding author. E-mail: w_avansi@if.sc.usp.br. Tel: +55 16 3373-9828.
† Universidade de São Paulo.
‡ Embrapa, Empresa Brasileira de Pesquisas Agropecuárias.
§ Universidade Federal de São Carlos.

10.1021/cg900373f CCC: $40.75
Published on Web 05/26/2009

Table 1. Experimental Conditions of the Samples Subjected to the Hydrothermal Treatment

sample	temperature (°C)	time (h)	pressure (MPa)
SAM01	60	6	0.3
SAM02	120	24	0.7
SAM03	180	2	1.3
SAM04	180	24	1.3
SAM05	200	24	1.7

releasing oxygen and leading to the formation of a decavanadic acid $[H_nV_{10}O_{28}]^{(6-n)}$ solution after a few hours. The decavanadic acid is then dissociated, resulting in the polymerization of the gel $V_2O_5 \cdot nH_2O$.[16] Li et al. obtained a bundle-like $V_2O_5 \cdot nH_2O$ using the $H_2O_2-V_2O_5$ route followed by hydrothermal treatment with the addition of inorganic ions. They showed that it is possible to obtain $V_2O_5 \cdot nH_2O$ at a relatively low temperature, 120 °C in 24 h, only in the presence of Co^{2+} ions. Moreover, they also showed that the presence of Co^{2+} can induce homogeneous nucleation of $V_2O_5 \cdot nH_2O$ cluster and favor the growth rate.[31]

To the best of our knowledge, this is the first time an evaluation is made of the effect of intrinsic parameters that can be controlled during hydrothermal treatment, such as temperature and time, in the evolution of vanadate species. Thus, this paper reports on a systematic study of the synthesis of $V_2O_5 \cdot nH_2O$ nanoparticles using the $H_2O_2-V_2O_5$ route by a template-free hydrothermal method without the addition of organic surfactant or inorganic ions. We show that it is possible through this "easy" and "clean" methodology to obtain $V_2O_5 \cdot nH_2O$ nanocrystals with controlled morphology and crystal structure. The amount of H_2O molecules between the layered structure and interplanar distance, *d*, also could be controlled in this method only through the correct control of the hydrothermal treatment variables.

Experimental Section

Solutions containing 0.06 M of peroxovanadate were prepared by dissolving V_2O_5 powder in distilled water with 30% of H_2O_2.The amount of H_2O_2 was set at a molar ratio of 1:10 (V/H_2O_2). The formation of a clear yellow solution after 10 min indicated the formation of vanadium peroxide.[16] The solution was placed into a microcontrolled hydrothermal cell with fine control of the temperature and monitoring of the self-generated pressure. After the treatment, the sample was rapidly quenched in an ice bath. Two synthesis variables were investigated: temperature and heat treatment time. The temperatures studied ranged from 60 to 200 °C, and the heat treatment time ranged from 2 to 24 h. Table 1 lists the experimental conditions of temperature, heat treatment time, and pressure reached during the synthesis.

The water content in the samples was investigated by thermal gravimetric analysis (TGA) using a TG 209 NETZSCH thermomicrobalance in a N_2 atmosphere from room temperature to 500 °C at a heating rate of 10 °C/min. To analyze the thermal properties of the samples after the above-described hydrothermal treatment, the samples were heat-treated at 50 °C to produce a powder sample.

The long-range order of the samples' structure was investigated by X-ray diffraction (XRD) using a Rigaku D/Max-2500PC diffractometer, with Cu Kα ($\lambda = 1.5406$) radiation. The crystallographic phase of the samples was also checked by using a micro-Raman microscope (WITec, Alpha 300S-CRM200). The spectral excitation was provided by an Ar^+ ion laser using the 514.5 nm laser line and 0.6 mW laser power. A low power laser was used to prevent the laser beam from changing the characteristics of the samples.[32] For these characterizations, the samples were deposited directly on sheet glass.

The variation in the electronic and local atomic structure was checked by X-ray absorption spectroscopy (XAS). The X-ray absorption near edge structure (XANES) region of the absorption spectra was measured at the V *K*-edge using the D08B-XAFS2 beamline at the Brazilian Synchrotron Light Laboratory (LNLS). The vanadium *K*-edge XANES spectra were collected in transmission mode at room temperature using a Si (111) channel-cut monochromator. The XANES spectra were measured from 40 eV below and 80 eV above the edge, with an energy step of 0.3 eV near the edge region. XANES spectra of the samples, which were deposited on polymeric membranes, were collected with the sample placed at 90° in relation to the X-ray beam. To provide good energy reproducibility during the collection of XANES data, the energy calibration of the monochromator was checked while the data were being collected, using a V metal foil.

The size and morphology of the vanadium oxide nanoparticles were determined using a Zeiss VP Supra 35 field emission scanning transmission electron microscope (FE-STEM) and a JEOL JEM-3010 microscope (300 KeV, 1.7 Å point resolution).

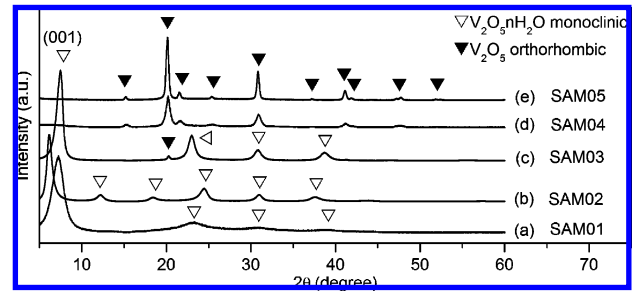

Figure 1. (a−e) XRD patterns of the as-prepared samples: SAM01 (60 °C for 6 h), SAM02 (120 °C for 6 h), SAM03 (180 °C for 6 h), SAM04 (180 °C for 24 h), and SAM05 (200 °C for 24 h).

Results and Discussion

Two synthesis variables were investigated: temperature and heat treatment time. The temperatures studied ranged from 60 to 200 °C and the heat treatment time ranged from 2 to 24 h. Table 1 lists the experimental conditions of temperature, heat treatment time, and pressure reached during the synthesis.

The formation of $V_2O_5 \cdot nH_2O$ nanoparticles was first detected at 60 °C after 6 h of treatment, and these nanoparticles are called SAM01. Figure 1 shows the XRD pattern of the as-prepared samples.

The XRD patterns of SAM01, SAM02, and SAM03 samples display a series of *00l* diffraction peaks, indicating a preferential orientation in the *c* direction. These diffraction peaks could be indexed as the $V_2O_5 \cdot nH_2O$ monoclinic phase.[25] The interlayer spacings *d* in the $V_2O_5 \cdot nH_2O$ structure were calculated from the (001) diffraction peak, and were 12.2 and 14.3 Å for samples SAM01 and SAM02, respectively. Unlike previous works, our results show that it is possible to obtain the $V_2O_5 \cdot nH_2O$ phase below 120 °C by heat-treating for 24 h and that the basal distance can be controlled simply by changing the temperature and time of hydrothermal treatment.[31] The sample treated at 180 °C for 6 h (SAM03) shows the presence of *00l* diffraction peaks, like those in SAM01 and SAM02 shown in the XRD patterns, as well as an additional peak around 20°. This additional peak could be indexed as the (001) diffraction peak belonging to the V_2O_5 orthorhombic phase (JCPDS card 85-0601). The interlayer spacing *d* for this sample was 12.2 Å, like that of sample SAM01. All the diffraction peaks of the sample treated at 180 °C for 24 h (SAM04) and that treated at 20 °C for 24 h (SAM05) were indexed as the V_2O_5 orthorhombic phase (JCPDS card 85-0601).

The water content and thermal stability of the samples were investigated by thermal gravimetric analysis (TGA). The TGA curves shown in Figure 2 indicate the existence of three dehydration steps for SAM01, SAM02, and SAM04, which are consistent with the literature.[21,32]

An analysis of the TGA curves indicated that, at room temperature, SAM01, SAM02, SAM04, and SAM05 contained,

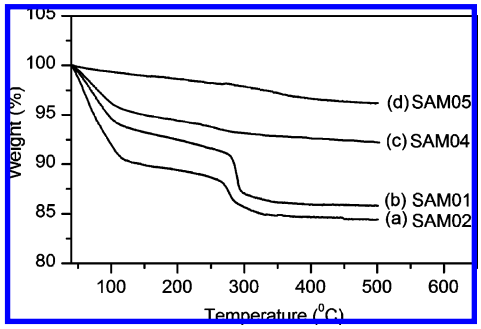

Figure 2. TGA curves for the samples: (a) SAM01, (b) SAM02, (c) SAM04, and (d) SAM05.

Table 2. Value of Basal Distance (*d*) and Amount of H_2O Molecules (*n*) for the Samples Indexed As $V_2O_5 \cdot nH_2O$ Monoclinic Phase

sample	*d* (A)	*n*
SAM01	12.2	1.8
SAM02	14.3	2.1

respectively, 1.8, 2.1, 1.0, and 0.5 mol of water in relation to the amount of V_2O_5. The TGA curve of SAM01 shows a loss of weakly bound and adsorbed water occurring over a wide range of temperatures up to 110 °C. The treatment of this sample at 110 °C produced the $V_2O_5 \cdot 1.0H_2O$ composition. Heating the same sample to 280 °C resulted in the $V_2O_5 \cdot 0.5H_2O$ composition through the elimination of bound water. Heating above this temperature induced loss of the remaining tightly bound water and crystallization of the material in the dehydrated orthorhombic phase.[32] The TGA profile of SAM02 differed slightly from that of SAM01 with regard to the *n* quantity. SAM03 was not subjected to TGA analysis due to the existence of two crystalline phases. As for the samples indexed as V_2O_5 orthorhombic phase, SAM04 and SAM05, the analysis of the TGA curves revealed the existence of a relatively small amount of water in the structure, that is, $n = 1.0$ and $n = 0.5$ mol, respectively. Although the XRD patterns of these two samples were indexed as V_2O_5 orthorhombic phase, that is, a dehydrated form, the TGA indicated that the structure of these samples contained a small quantity of H_2O molecules, forming the $V_2O_5 \cdot 1.0H_2O$ (SAM04) and $V_2O_5 \cdot 0.5H_2O$ (SAM05) compositions. SAM04 also showed three stages of dehydration, but showed various differences from samples SAM01 and SAM02. The treatment of SAM04 at the same temperatures yielded a sample with a different amount of *n* than that of SAM01 and SAM02. The loss of weakly bound and adsorbed water also occurred over a wide range of temperatures up to 110 °C. However, when the sample was annealed at this temperature, a composition was formed whose structure contained 0.4 mol of H_2O molecules per mole of vanadium pentoxide. Heating to 240 °C led to the removal of bound water, resulting in a sample containing 0.2 mol of H_2O molecules per mole of vanadium pentoxide. Above this temperature, the remaining tightly bound water is removed.[32] Unlike the other samples, the TGA profile of SAM05 showed a continuous loss of water up to 350 °C.

With regard to samples indexed as $V_2O_5 \cdot nH_2O$ monoclinic phase, according to Livage et al., the increase in the amount of water molecules is related to the increase in basal distance. Table 2 summarizes the values of basal distance, *d*, and the amount of H_2O molecules, *n*, for the samples indexed as $V_2O_5 \cdot nH_2O$ monoclinic phase (SAM01 and SAM02). The dependence on *d* and *n* can also be observed from the results are presented in Table 2.

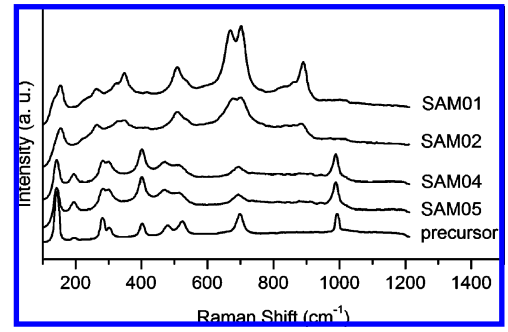

Figure 3. Micro-Raman spectra of the as-prepared samples: SAM01 (60 °C for 6 h), SAM02 (120 °C for 6 h), SAM04 (180 °C for 24 h), and SAM05 (200 °C for 24 h).

The samples treated from 120 to 180 °C for 2 h showed no detectable change in the basal distance or in the amount of H_2O molecules. The XRD results of SAM03 indicated that the layered phase possessed the same basal distance as the sample obtained at 60 °C (SAM01). Thus, according to the findings of Livage et al. and to what we observed in our own samples, the amount of water in SAM03 is expected to decrease, indicating a loss of water molecules embedded in the structure. Upon increasing the treatment time to 24 h (SAM04), the TGA profiles revealed a small quantity of water molecules in the structure. These results indicate that the interlayer water is removed continuously up to 24 h, when a change in the structure can be detected. Our results show that the as-synthesized samples became dehydrated after the formation of the $V_2O_5 \cdot nH_2O$ monoclinic. The samples treated at 200 °C showed the same dehydration process beginning at 2 h, and after 24 h of treatment, a smaller amount of water molecules was detected than in SAM04. Through this, the quantity of water molecule in the structure was found to decrease as the temperature increased. Zhou et al. observed a similar dehydration process using a stronger oxidant to remove H_2O molecules from the structure.[30]

Several works discuss the importance of the amount of water in the structural properties of $V_2O_5 \cdot nH_2O$.[2,3,10,12,14,19] Our results demonstrated that the amount of water can be controlled easily by changing the hydrothermal conditions, temperature and time of treatment. Moreover, our results also indicated the possibility of obtaining nanostructures with smaller amounts of H_2O molecules at lower temperatures than when a post-thermal treatment is applied. The solubility of the oxide is highly improved in hydrothermal conditions, but the self-generated pressure in the reactor can affect phase stability. We also found that the dehydrated form of V_2O_5 is more stable in these conditions, since this phase stabilized spontaneously.

Figure 3 shows the micro-Raman spectra of the oxide precursor and samples SAM01, SAM02, SAM04, and SAM05. The oxide precursor spectra showed bands at 144, 196, 283, 303, 404, 480, 525, 700, and 994 cm^{-1}, corresponding to the crystalline V_2O_5 orthorhombic phase.[33,34] The Raman spectra of SAM01 and SAM02 presented bands at 158, 262, 322, 348, 507, 665, 704, and 890 cm^{-1}, which differed from those of the oxide precursor. According to Abello et al., the change in these bands when compared with the V_2O_5 orthorhombic phase is due to the presence of water molecules between the layers, which modifies the structure of the samples.[33] SAM04 and SAM05 showed Raman spectra very similar to that of the precursor, indicating that the structure resembled that of the V_2O_5 orthorhombic phase, which was consistent with our XRD results.

X-ray absorption spectroscopy (XAS) was employed to characterize the local order and the electronic structure of the samples.

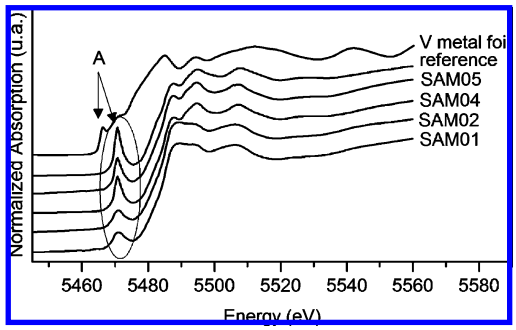

Figure 4. Normalized vanadium K-edge XANES spectra of reference compounds (V_2O_5 orthorhombic phase and V metal foil) and the as-prepared SAM01, SAM02, SAM04, and SAM05 samples.

Table 3. Energy Position and Intensity of Pre-Edge and Edge Features of Studied Samples, Vanadium Metal Foil and Orthorhombic V_2O_5 Reference Sample

sample	E_{edge}[a] (eV)	E_A[b] (eV)	I_p[c] intensity	E_A*[d] (eV)
SAM01	5481.9	5470.9	0.19	5469.4
SAM02	5481.9	5470.9	0.18	5469.1
SAM04	5481.7	5470.6	0.35	5469.7
SAM05	5481.9	5470.9	0.33	5469.7
V_2O_5 (reference)	5481.4	5470.9	0.47	5469.7
V metal	5473.2	5465.4	0.26	5467.9

[a] Energy measured at half-height of the normalized XANES spectra. [b] Energy of pre-edge peak. [c] Intensity of pre-edge peak. [d] Energy from the point of inflection of the pre-edge peak, indicated by the arrow, determined by the first derivative of the normalized XANES spectrum.

Figure 4 shows the normalized XANES spectra of V_2O_5 orthorhombic phase and V metal foil, used as a reference compounds, and normalized XANES spectra of the SAM01, SAM02, SAM04, and SAM05 samples. Note that the XANES spectra were taken with the samples oriented at a 90° angle to the X-ray beam and X-ray polarization effects were not considered.

The XANES spectra of SAM01 and SAM02 in Figure 4 indicate that increasing the heat treatment from 60 °C (SAM01) to 120 °C (SAM02) did not give rise to any significant change in these spectra. On the other hand, when the samples were treated at 180 and 200 °C (SAM04 and SAM05), the XANES spectra revealed some differences in the pre- and postedge region. In fact, the XANES spectra of these two samples were generally similar to the V_2O_5 reference compound, although the pre-edge peak *A* showed lower intensity.

The pre-edge peak is a product of the transition from V 1s states to V 3d states. This transition, however, is forbidden by the dipole selection rules in centrosymmetric systems, although it is allowed in noncentrosymmetric systems via hybridization between the V 3d and O 2p states. The intensity of the pre-edge peak showed a strong dependence on the local structure around vanadium atoms, indicated by the degree of distortion of the first oxygen atoms, which influenced the degree of hybridization between the O 2p and V 3d orbitals. The degree of hybridization increased as the V=O distance decreased.[21]

We found that the intensity of the pre-edge peak *A* increased along with the temperature, but was lower than that of the V_2O_5 reference compound, as can be observed in Table 3. According to the literature, an increase in the pre-edge peak intensity suggests a decrease in the vanadyl (V=O) distance, which increases the degree of distortion of the local structure, thus decreasing the local symmetry of the structure within the VO_5 square pyramid.[21] Therefore, the lower intensity of the pre-edge peak in SAM01 and SAM02 indicates that the local structure of V in the $V_2O_5 \cdot nH_2O$ samples has a higher degree of symmetry within the VO_5 square pyramid when obtained at lower temperatures.

Figure 5a offers a magnified view of the pre-edge region of the samples of this study in comparison with the V_2O_5 reference compound. Table 3 shows the energy position and the normalized intensity of the pre-edge peak *A*, as well as the edge energy which was calibrated using a vanadium metal foil ($E = 5465.4$ eV).

The edge energy, E_{edge}, like the pre-edge peak energy in all the samples, Figure 4, is similar to that of the V_2O_5 orthorhombic phase, Table 3. The values of the energy position of the E_{edge} of all the samples were determined from the normalized absorption at half-height. The energy of the inflection point at the onset of the pre-edge peak or the main edge is also sensitive to variations in the oxidation state of vanadium.[21] SAM01 and SAM02 showed a peak shifting toward a lower energy and a broadening when compared to the reference compound. This shift was estimated to be 0.3 and 0.6 eV (Table 3), respectively, in SAM01 and SAM02. This result suggests that the vanadium atoms in the $V_2O_5 \cdot nH_2O$ samples with a monoclinic phase were in a mixed-valence state (V^{4+} and V^{5+}), with a large amount of V^{4+} in SAM02. According to Livage et al., the larger amount of V^{4+} ions in SAM02 may be associated with the amount of H_2O molecules present in the layered structure, and are therefore related to the increase in *d* interlayer spacing, a dependence that can be observed in Table 2.[21]

Mansour et al. used XAS to measure the oxidation state of vanadium atoms in samples of $V_2O_5 \cdot nH_2O$ aerogels and ambigels with $n = 2.0$, 1.0, and 0.5. According to their findings, only the sample with $n \approx 0.5$ showed the presence of V^{4+}, whose concentration was estimated at 0.29 and 0.26 for the aerogel and ambigel samples, respectively.[21] In our case, the SAM04 and SAM05 results presented in Table 3 and Figure 5b indicate that the energy position of the pre-edge peak and the vanadium edge and the first derivative of the pre-edge region were quite similar to orthorhombic V_2O_5. This indicates that the oxidation state of vanadium atoms in the samples under study were similar to the vanadium atoms in the reference compound, that is, V^{5+}. However, using the EPR technique, Livage et al. showed that $V_2O_5 \cdot nH_2O$ samples could contain about 1% of V^{4+}.[15] Therefore, although we could not eliminate the presence of a small amount of V^{4+} in our SAM04 and SAM05 samples, we can state, based on our XANES spectra, that the valence of the vanadium atoms was preferentially 5+.

With regard to the post-edge region, the XANES spectra of SAM04 and SAM05 presented three peaks, as observed in the spectrum of the reference compound (V_2O_5 orthorhombic phase) shown in Figure 4. This suggests that the structure around V is quite similar to the precursor, which is in good agreement with the XRD patterns and micro-Raman spectra. On the other hand, the postedge regions of the XANES spectra of SAM01 and SAM02 presenting a $V_2O_5 \cdot nH_2O$ monoclinic phase were completely distinct. These spectra had a smooth aspect, indicating greater disorder around the vanadium atoms.[35]

The samples' morphology was investigated by field emission scanning transmission electron microscopy (FE-STEM). Figure 6a shows that the sample obtained at 60 °C for 6 h (SAM01) was composed of 20−30 nm wide ribbons. This morphology resembles that of the samples synthesized at 120 °C (not shown in this image). At a temperature of 180 °C and 6 h of treatment (SAM03), the FE-STEM image revealed the presence of two morphologies, nanoribbons and nanowires, Figure 6b, confirming what was observed in the XRD patterns. Increasing the treatment time of SAM04 resulted in a nanostructure composed only of 20−30 nm wide nanowires, Figure 6c. The sample

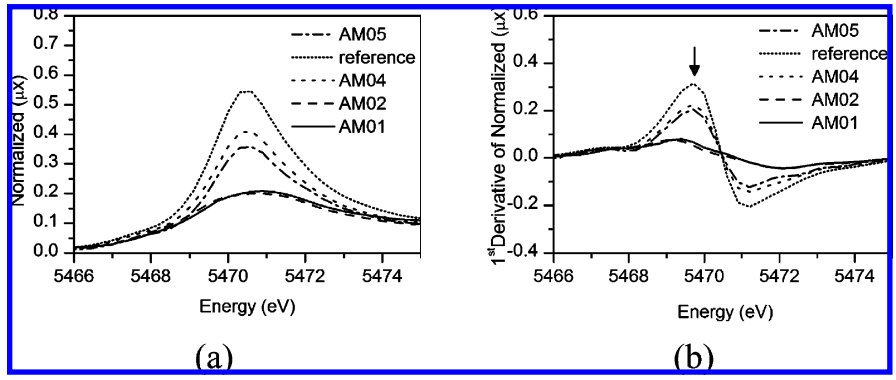

Figure 5. (a) The expanded view of the pre-edge region of normalized XANES and (b) an expanded view of the first derivative of the pre-edge region for the samples SAM01, SAM02, SAM04, SAM05, and orthorhombic V_2O_5 as reference compound.

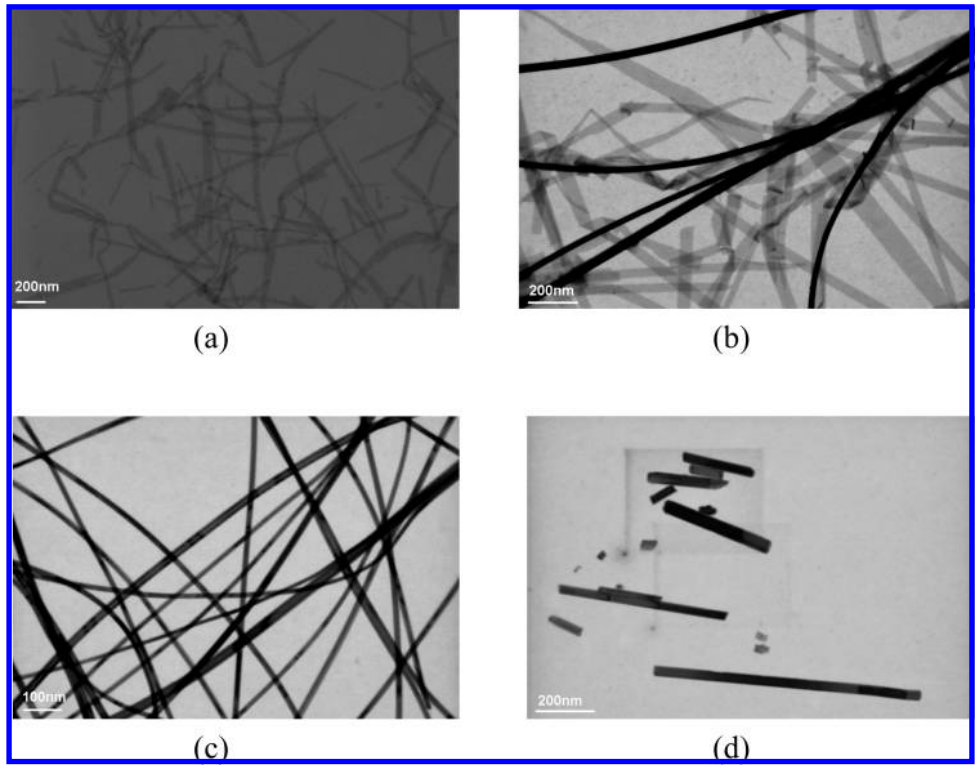

Figure 6. FE-STEM images of the samples: (a) SAM01, (b) SAM03, (c) SAM04, and (d) SAM05.

treated at 200 °C for 6 h possessed the same structure (not shown here); however, extending the treatment time of SAM05 to 24 h led to slight morphological changes, such as 30−40 nm wide rods. These morphologies were quite similar to those reported by various authors using different methods of synthesis followed by hydrothermal treatment.[3,28,30] Nevertheless, Zhou et al. reported the synthesis of nanowires with a diameter of about 60−70 nm, while SAM04 in the experimental condition showed a diameter of about 20−30 nm. The FE-STEM images of SAM05 revealed a nanorod morphology with a diameter larger than that of SAM04, that is, about 40 nm. The FE-STEM images also indicated that the nanoparticles obtained at 180 °C (SAM04) were more flexible than the sample obtained at 200 °C (SAM05). This behavior may be ascribed to the larger amount of H_2O molecules in the structure. Unlike some reports, which found that the amount of H_2O molecules was related directly to the distance *d* while maintaining the same ribbon morphology, our work shows that the amount of H_2O molecules appears to be related to the morphology.[2,12,14,15]

On the basis of the experimental results, the formation process of orthorhombic $V_2O_5 \cdot nH_2O$ nanowires and nanorods appears to be related to the process of dehydration of the monoclinic $V_2O_5 \cdot nH_2O$ nanoribbons, through control of temperature and time of treatment.

The HRTEM image of SAM01 is shown in Figure 7a,b. Figure 7b indicates that the lattice parameter is about 0.36 nm. This distance is consistent with the [010] plane of the orthorhombic structure, indicating that these nanoribbons grow along the (010) direction. This result was expected, for according to the XRD results, the presence of water in the lamellar structure causes a significant change, mainly in the *c* direction.[33]

The HRTEM image of SAM05 in Figure 8a,b shows a nanowire with a $V_2O_5 \cdot 0.5H_2O$ orthorhombic phase. Consistent with the XRD results, this figure shows a more ordered structure than the $V_2O_5 \cdot 1.8H_2O$ monoclinic phase. The distance between neighboring planes is about $b = 0.36$ nm along the nanowire's diameter and about $a = 0.64$ nm along its length. These distances are consistent with the (010) and (200) planes,

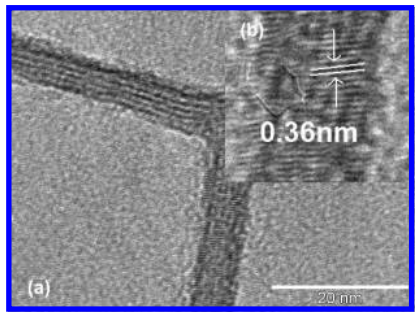

Figure 7. (a) and (b) HR-TEM images of the sample obtained at 60 °C for 6 h (SAM01).

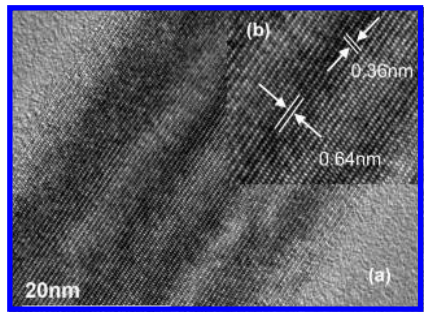

Figure 8. (a) and (b) HR-TEM images of the sample obtained at 200 °C for 24 h (SAM05).

respectively, in the V_2O_5 orthorhombic phase, as observed in the XRD pattern. The lattice space relative to the (010) plane is similar to that measured in the ribbon-like nanoparticles (SAM01), which presents a larger amount of H_2O molecules, as expected. The HRTEM images in Figures 7b and 8b confirm the good single-crystal nature of SAM01 and SAM05.

The results reported here indicate that, in hydrothermal conditions, nanocrystals with different structures and morphologies can be obtained without adding any other elements to the synthesis, simply by controlling the treatment temperature and time, resulting in nanomaterials for potential use in a variety of applications.

Conclusion

Using a hydrothermal method based on the decomposition of vanadium peroxide, $V_2O_5 \cdot nH_2O$ nanostructures were synthesized with different amounts of water molecules, resulting in distinct morphologies and structures. Our results indicate that, unlike several studies that discuss the important role of additives or reducing species in the synthesis of $V_2O_5 \cdot nH_2O$ nanoparticles, we successfully synthesized these nanocrystalline forms simply by controlling the hydrothermal parameters, that is, temperature and time, with self-generated pressure. The fine control of these parameters seems to be the key factor to obtain the desired nanomaterial. At high hydrothermal temperatures, the less hydrated form of vanadium pentoxide was shown to be more stable, despite the higher solubility of the oxide in this condition. This suggests that self-generated pressure plays a role in the crystallization process. The formation of the $V_2O_5 \cdot nH_2O$ orthorhombic phase in the nanowire and nanorod forms was developed by the dehydration of the $V_2O_5 \cdot nH_2O$ monoclinic phase, following a sequence of phase transformation. This dehydration and the resulting change in the structure of the as-synthesized samples did not alter the oxidation state of vanadium in the samples with $V_2O_5 \cdot nH_2O$ orthorhombic phase when compared with the precursor. Nevertheless, the $V_2O_5 \cdot nH_2O$ monoclinic phase showed the presence of a mixed valence of vanadium atoms. The local structure around the vanadium atoms in the samples with $V_2O_5 \cdot nH_2O$ monoclinic phase displayed a higher degree of symmetry within the VO_5 square pyramid structure, albeit with a more disordered medium range order than that of the samples containing $V_2O_5 \cdot nH_2O$ orthorhombic phase.

Acknowledgment. The authors gratefully acknowledge the financial support of the Brazilian research funding agencies FAPESP and CNPq. XANES measurements and HRTEM microscopy facilities were provided by LNLS-Campinas, SP, Brazil.

References

(1) Karunakaran, C.; Senthilvelan, S. J. *Colloid Interface Sci.* **2005**, *289*, 466.
(2) Livage, J. *Chem. Mater.* **1991**, *3*, 578.
(3) Liu, J.; Wang, X.; Peng, Q.; Li, Y. *Adv. Mater.* **2005**, *17*, 764.
(4) Serier, H.; Achard, M.-F.; Babot, O.; Steunou, N.; Maquet, J.; Livage, J.; Leroy, C.; Backov, R. *Adv. Funct. Mater.* **2006**, *16*, 1745.
(5) Leroy, C. M.; Achard, M. F.; Babot, O.; Steunou, N.; Masse, P.; Livage, J.; Binet, L.; Brun, N.; Backov, R. *Chem. Mater.* **2007**, *19*, 3988.
(6) Raju, A. R.; Rao, C. N. *J. Chem. Soc.* **1991**, *18*, 1260.
(7) Imawan, C.; Steffes, H.; Solzbacher, F.; Obermeier, F. *Sens. Actuators B* **2001**, *77*, 346.
(8) Cantu, M.; Gomez-Romero, P. J. *Electrochem. Soc.* **1999**, *146*, 4139.
(9) Li, X.; Li, W.; Ma, H.; Chen, J. *J. Electrochem. Soc.* **2007**, *154*, A39.
(10) Li, B.; Xu, Y.; Rong, G.; Jing, M.; Xie, L. *Nanotechnology* **2006**, *17*, 2560.
(11) Krusin-Elbaum, L.; Newns, D. M.; Zeng, H.; Derycke, V.; Sun, J. Z.; Sandstrom, R. *Nature* **2004**, *431*, 672.
(12) Wang, Y.; Cao, G. *Chem. Mater.* **2006**, *18*, 2787.
(13) Ivankovic, S.; Music, S.; Gotic, M.; Ljubesĭc, N. *Toxicology in Vitro* **2006**, *20*, 286.
(14) Livage, J. *Mater. Res. Bull.* **1991**, *26*, 1173.
(15) Livage, J. *Coord. Chem. Rev.* **1998**, *180*, 999.
(16) Alonso, B.; Livage, J. *J. Solid State Chem.* **1999**, *148*, 16.
(17) Holland, G. P.; Huguenin, F.; Torresi, R. M.; Buttry, D. A. *J. Electrochem. Soc.* **2003**, *150*, 721.
(18) Chandrappa, G. T.; Steunou, N.; Cassaignot, S.; Bauvais, C. *J. Sol-Gel Sci. Technol.* **2003**, *26*, 593.
(19) Wang, Y.; Shang, H.; Chou, T.; Cao, G. *J. Phys. Chem. B* **2005**, *109*, 11366.
(20) Mansour, A. N.; Smith, P. H.; Balasubramanian, M.; Mcbreen, J. *J. Phys. Chem. B* **2005**, *109*, 16700.
(21) Mansour, A. N.; Smith, P. H.; Balasubramanian, M.; Mcbreen, J. *J. Electrochem. Soc.* **2005**, *152*, 13112.
(22) Huang, C.; Liu, X.; Kong, L.; Zhou, H.; Liu, Y.; Qiu, J.; Wang, Y. *Rare Metals* **2006**, *25*, 88.
(23) Pinna, N.; Wild, U.; Urban, J.; Schlogl, R. *Adv. Mater.* **2003**, *15*, 329.
(24) Ponzio, E. A.; Benedetti, T. M.; Torresi, R. M. *Electrochim. Acta* **2007**, *52*, 4419.
(25) Petkov, V.; Trikalitis, P. N.; Bozin, E. S.; Billinge, J. L.; Vogt, T.; Kanatzidis, G. M. *J. Am. Chem. Soc.* **2002**, *124*, 10157.
(26) Krumeich, F.; Muhr, H. J.; Niederberger, M.; Bieri, F.; Gunther, D.; Nesper, R. *J. Am. Chem. Soc.* **1999**, *121*, 8324.
(27) Niederberger, M.; Muhr, H. J.; Krumeich, F.; Bieri, F.; Gunther, D.; Nesper, R. *Chem. Mater.* **2000**, *12*, 1995.
(28) Gao, S.; Chen, Y.; Luo, H.; Jiang, L.; Ye, B.; Wei, M.; Wei, K. J. *J. Nanosci. Nanotechnol.* **2008**, *8*, 3500.
(29) Pan, D.; Shuyuan, Z.; Chen, Y.; Hou, J. G. *J. Mater. Res.* **2002**, *17*, 1981.
(30) Zhou, F.; Zhao, X.; Yuan, C.; Li, L. *Cryst. Growth Des.* **2008**, *8*, 723.
(31) Li, G.; Jiang, L.; Peng, H. *Mater. Lett.* **2007**, *61*, 4070.
(32) Souza Filho, A. G.; Ferreira, O. P.; Santos, J. G.; Mendes Filho, J.; Alves, O. L. *Nano Lett.* **2004**, *4*, 2099.
(33) Abello, A.; Husson, E.; Repelin, Y.; Lucazeau, G. *J. Solid State Chem.* **1985**, *56*, 379.
(34) Chou, J. Y.; Lensch-Falk, J. L.; Hemesath, E. R.; Lauhon, L. J. *J. Appl. Phys.* **2009**, *105*, 034310.
(35) Nabavi, M.; Taulelle, F.; Sanscwez, C.; Vprdacwer, M. *J. Phys. Chem. Solids* **1990**, *51*, 1375.

CG900373F